Low Power Radiometric Partial Discharge Sensor using Composite Transistor-Reset Integrator

David W. Upton, Bakhtiar I. Saeed, Peter J. Mather, Martin J. N. Sibley, Pavlos I. Lazaridis, Keyur K. Mistry and **Ian A. Glover**
University of Huddersfield,
Department of Engineering and Technology
Huddersfield HD1 3DH, UK

Flávio Torres Filho
Instituto Federal da Paraiba/ Campus Patos
Department of Electrotechnics
58700-000 Patos, PB, Brazil

Christos Tachtatzis and **Robert C. Atkinson**
University of Strathclyde
Glasgow G1 1XW, UK

Martin D. Judd
High-Frequency Diagnostics and Engineering Ltd
Glasgow G14 0BX, UK

ABSTRACT

The measurement of partial discharge provides a means of monitoring insulation health in high-voltage equipment. Traditional partial discharge measurements require separate installation for each item of plant to physically connect sensors with specific items. Wireless measurement methods provide an attractive and scalable alternative. Existing wireless monitoring technologies which use time-difference-of-arrival of a partial discharge signal at multiple, spatially separated, sensors place high demands on power consumption and cost due to a requirement for rapid sampling. A recently proposed partial discharge monitoring system using a wireless sensor network and measuring received signal strength only, has potential cost and scalability advantages. An incoherent wireless sensor incorporating a transistor-reset integrator has been developed that reduces the measurement bandwidth of the PD events and alleviates the need for high-speed sampling. It is based on composite amplifier techniques to reduce the power requirements by a factor of approximately four without compromising precision. The accuracy of the proposed sensor is compared to that obtained using a high-speed digital sampling oscilloscope. Received energies were measured over a 10 m distance in 1 m increments and produced an error within 1 dB beyond 4 m and 3.2 dB at shorter distances, resulting in a measurement accuracy within 1 m.

Index Terms — **Analog processing circuits; partial discharge measurement; power system reliability; UHF measurements; wireless sensor networks.**

1 INTRODUCTION

PARTIAL discharge (PD) occurs in degraded high voltage (HV) insulation. The IEC60270 standard defines PD as "a localized electrical discharge that only partially bridges the insulation between conductors and which can or cannot occur adjacent to a conductor. Partial discharges are in general a consequence of local electrical stress concentrations in the insulation or on the surface of the insulation. Generally, such discharges appear as pulses having a duration of much less than 1 microsecond" [1]. Overtime the discharge can further degrade the insulation, leading to eventual catastrophic failure. Each discharge represents a short current pulse and the monitoring of these pulses is a well-established technique for assessing the insulation condition in HV equipment such as transmission lines, switchgear and transformers [2]. Traditional technologies for detecting PD current pulses include galvanic contact devices, high frequency current

Manuscript received on 7 December 2017, in final form 5 February 2018, accepted 5 February 2018. Corresponding author: D. Upton.

DOI: 10.1109/TDEI.2018.007253

transformers (HFCTs) and transient earth voltage (TEV) sensors [3]. These techniques provide direct access to PD events, along with valuable information, such as apparent charge and spectra, in order to evaluate the type of discharge and assess the fault progression. Due to the close coupling of the sensor and PD source, however, they are sensitive to only the most local sources of PD, requiring separate sensor provision for each item of plant to be monitored. Comprehensive monitoring of all plant items in a large substation using these technologies can be expensive due to the large number of sensors required and the extensive wiring harness needed to connect the sensors to a data collection hub. The resulting sensor network can also be expensive to reconfigure.

Radiometric detection of PD uses a broadband radio receiver to detect the UHF energy radiated electromagnetically from the source of the PD discharge. Multiple, spatially-separated, radiometric sensors can be used to locate the PD source. It is a non-invasive, easy to install and simple to reconfigure technique, and provides an attractive alternative to traditional approaches since no galvanic or physical connection is necessary and a single sensor can monitor multiple items of plant equipment. A limitation of wireless techniques is, however, potentially reduced diagnostic information, since the PD signal is degraded due to the radiation process, and further distorted by the propagation environment. Several variations on radiometric PD detection methods have been suggested [e.g. 4-6]. These include techniques which directly sample the RF PD signal [7-9]. Whilst direct sampling provides a particularly accurate measurement of the signal, and is necessary if the PD source is to be located using time of arrival (TOA) or time difference of arrival (TDOA) measurements, it requires a sampling rate of the order of 1 GSa/s typically, leading to a power in excess of 300 mW. The sensors in a practical PD wireless sensor network (WSN) should be capable of operating for at least a year between battery changes. Low power techniques using peak hold circuitry have already been described [10]. Directly sampled peak hold circuits for radiometric measurements are complicated to implement due to the short duration of the received PD signal peak. Achieving linearity over the dynamic range is also difficult due to the non-linear response of the required rectifying diodes. Furthermore, whilst peak power provides an acceptable metric for localization, it is not easily related to apparent charge in the PD fault [11] making diagnostic analysis difficult.

Measurements have been reported [12, 13] that suggest total RF energy propagated from a PD discharge and apparent charge displaced in the void have a linear relationship; therefore, integration of received PD power may provide useful diagnostic information. Methods have been proposed for PD location and measurement using received signal-strength (RSS) in the UHF frequency band [14-16]. The benefit of RSS over TOA and TDOA based systems is that synchronization between nodes is not required, making a WSN fully-scalable for the area to be observed. However, the fundamental challenge of such an incoherent network of sensors is the wide bandwidth of the PD signal limiting the measurement signal-to-noise ratio (SNR) and thus the detection range. Some of these techniques use envelope detection in order to remove the RF component from the received signal [17] and allow for reduced sampling rates of around 20 MSa/s at the cost of reduced measurement accuracy [18].

A WSN system for the detection, location and monitoring of PD has previously been proposed [19-21]. The system is based around radiometric sensors that utilize a transistor-reset integrator (TRI), removing the requirement for high speed data conversion and data processing. Whilst conversion speed is reduced, power consumption is still an issue if precision high-speed analogue IC-based circuitry is used to detect and measure the PD signal. The TRI requires a low offset voltage, wide bandwidth and high input impedance in order to operate correctly. Furthermore, the sensor nodes (and therefore the TRI) must be capable of operating in an outdoor environment over a temperature range of -10 to +40 ºC without significant errors. A signal processing circuit based around a high-speed precision composite amplifier is proposed here that removes the requirement for high-speed direct conversion and high-speed signal processing whilst maintaining a large bandwidth and high precision. The quiescent current consumption of the proposed circuit is less than 10 mA, extending the time required between sensor node battery changes significantly. Battery life is further extended by placing the node into stand-by mode in between measurements, significantly reducing the supply current of the sensor nodes and increasing sensor operating time.

2 WIRELESS PD SENSOR NODE

2.1 SENSOR OVERVIEW

The sensor node, Figure 1, comprises a dipole antenna, an RF front-end, a signal conditioning unit, a micro-controller and a WirelessHART unit.

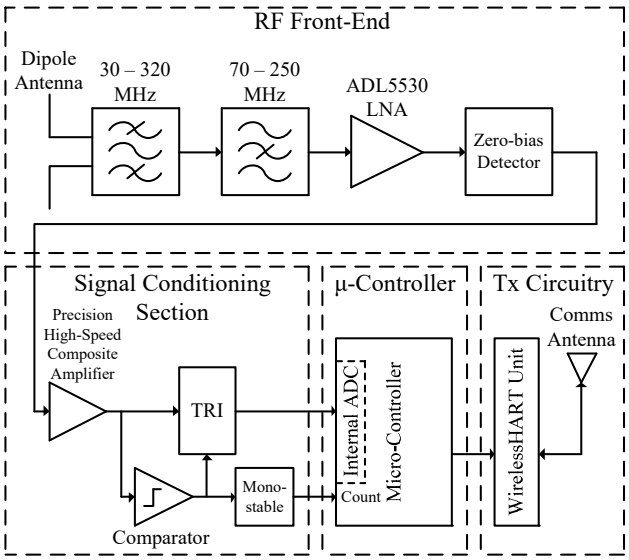

Figure 1. Radiometric PD sensor system diagram.

The RF front-end contains a band-pass roofing filter, a band-stop filter, low noise amplifier (LNA) and detector. Experimental work presented in [22, 23] found that the frequency ranges of a variety of radiometric PD typically reside between 50–800 MHz, with the majority of the energy below 300 MHz; therefore, the sensor measurement band was selected within this range. The roofing filter excludes all interference and noise outside the 30 – 320 MHz PD measurement band. The band-stop filter removes coherent interference in the region of 70 – 250 MHz (principally arising from FM radio, digital TV and DAB transmissions). The LNA provides a fixed gain of 16.5 dB to increase the sensor sensitivity. Due to the filters and LNA, the RF front-end has a frequency response with two main bands of approximately 30-70 MHz and 250-320 MHz, with a pass-band gain between 12-14 dB, and a noise figure in the range of 5-7 dB. The detector uses two HSMS2850 high sensitivity Schottky diodes in the voltage-doubler zero-bias circuit shown in Figure 2, and produces a baseband output voltage approximately proportional to the RF input power [24]. The output-input characteristic of the detector, shown in Figure 3, was generated by applying a sine-wave signal, at a frequency of 200 MHz, to the input of the detector and adjusting the power level of the signal from -25 to 0 dBm.

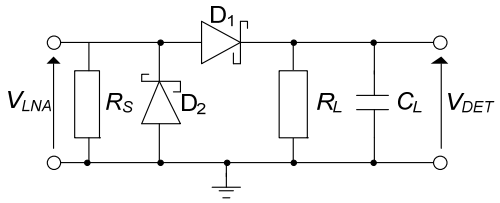

Figure 2. Zero-bias detector circuit, R_S provides a 50Ω input impedance. R_L is set to 1.5 kΩ to ensure the output tracks the envelope of the PD signal, and C_L is the 14 pF input capacitance of the oscilloscope used for measurement.

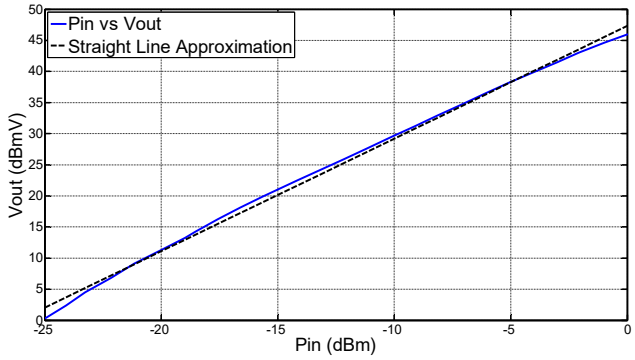

Figure 3. Detector output-input characteristic with straight line approximation.

V_{LNA} and V_{DET} are the LNA output voltage and detector output voltage respectively. The detector requires no power supply at the cost of reduced sensitivity and dynamic range. The straight line approximation transfer function is:

$$V_{DET} = KP_{IN} \quad (1)$$

where P_{IN} is the power of the received RF signal, V_{DET} is the detector output and K = 185 mV/mW. The signal conditioning unit comprises a high-speed, precision, non-inverting amplifier, a comparator and a transistor reset integrator (TRI). The non-inverting amplifier in Figure 1 presents a high impedance to the detector output ensuring that detector sensitivity is not reduced due to loading. The TRI provides further amplification and integrates the precision amplifier output giving a signal proportional to the accumulated energy of the PD RF pulses. Each additional pulse, therefore, produces a quasi-step change in the TRI output. The size of the step is a measure of PD pulse energy. Each step of the resulting staircase TRI output is sampled by the internal ADC of the micro-controller which calculates the delta step-size. The step increments are averaged to find the mean PD signal energy. A comparator channel driven by the non-inverting amplifier enables the TRI when PD is present. When PD is absent the output of the comparator disables the TRI avoiding integration when only noise is present. The comparator output also drives a mono-stable, with a 5 µs time-constant that produces a PD pulse count in the microcontroller. The 5 µs time-constant ensures that the micro-controller has sufficient time to detect the count pulse.

2.2 PROPOSED SIGNAL CONDITIONING CIRCUITRY

The precision high-speed amplifier provides a high input impedance to ensure minimal loading to the zero-bias detector, whilst the DC offset voltage and drift are kept to a minimum so that a low threshold voltage can be achieved by the comparator over a substantial ambient temperature range. These requirements would place too high a demand on a single operational amplifier so a composite design has been implemented [25, 26], Figure 4.

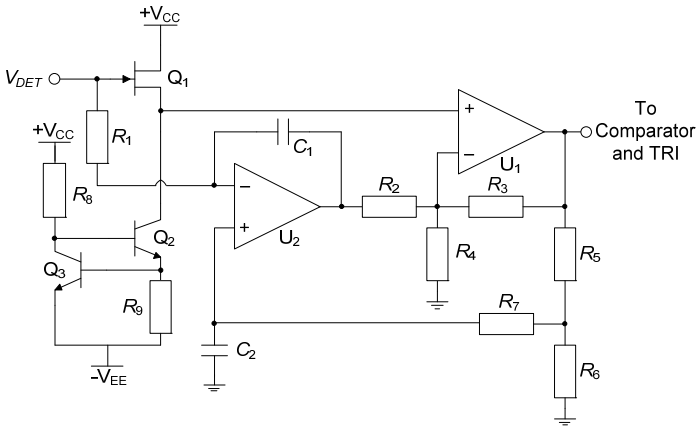

Figure 4. Precision high-speed composite amplifier.

The circuit is built around a 500 µA 105 MHz bipolar operation amplifier U_1 forming a non-inverting amplifier with R_3 and R_4 setting the closed loop voltage gain to 3.2. A discrete BF862 JFET source follower input stage provides a high impedance, low noise, input. The FET, Q_1, is biased at 500 µA via the V_{BE} referenced current source [27], Q_2 and Q_3. This arrangement would normally result in excessive offset voltage and temperature drift due to the JFET. The circuit attains its DC precision, however, through stabilization using U_2; an 18 µA, 3 µV offset, precision operational amplifier. This provides DC compensation for both the FET and the offset voltage of U_1.

The circuit operates as follows. A replica feedback point is created via R_5 and R_6. U_2 monitors the DC component of this

voltage through a low-pass filter (R_7 and C_2), with a cutoff frequency of 0.48 Hz to ensure the detected PD signal is fully removed, and compares it to the input DC voltage through an identical filter (R_1 and C_1). The output of U_2 then adjusts the DC level of U_1's summing junction to that of the V_{GS} bias voltage of Q_1, resulting in an output DC offset error equal to that of U_2 multiplied by the closed loop gain of U_1. Voltage offset temperature drift is also limited to that of U_2, (approximately 0.05 µV/ºC max). The maximum offset is thus limited to below 10 µV over a range of -10 to 40 ºC. The output of the precision high-speed amplifier is applied to a high-speed comparator, Figure 5, and the TRI.

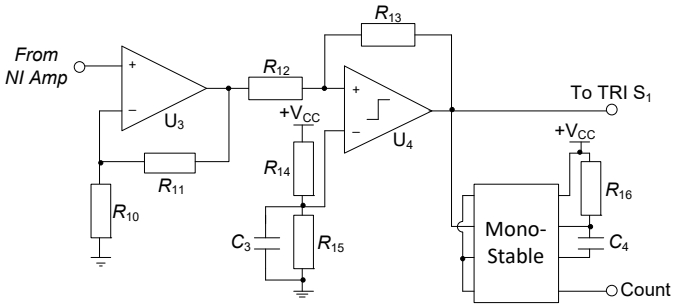

Figure 5. Precision high-speed comparator and mono-stable section.

The comparator is a low-power high-speed type, with a quiescent supply current of 470 µA and a propagation delay of 8 ns. High-speed non-inverting amplifier U_3, set to a gain of 10, increases the input signal allowing the comparator threshold to be set to a level significantly higher than the noise floor, ensuring reduced probability of false triggering. The comparator section is set to a threshold voltage of 4 mV (equating to a receiver sensitivity of -36 dBm at the receiving antenna), which activates the integration window of the TRI and triggers the mono-stable circuit. The mono-stable output pulse provides a digital count to the micro-controller every time a PD pulse is received. The timing components, R_{16} and C_4, set the 5 µs time-constant. Figure 6 shows the received emulated PD source, the detector output, the precision high-speed amplifier output and the comparator output, the delay to the amplifier output is due to the 150 V/µs slew-rate of U_1, and the transient oscillations at the peak and tail of the output waveform are due to the output of the high speed comparator switching transitions.

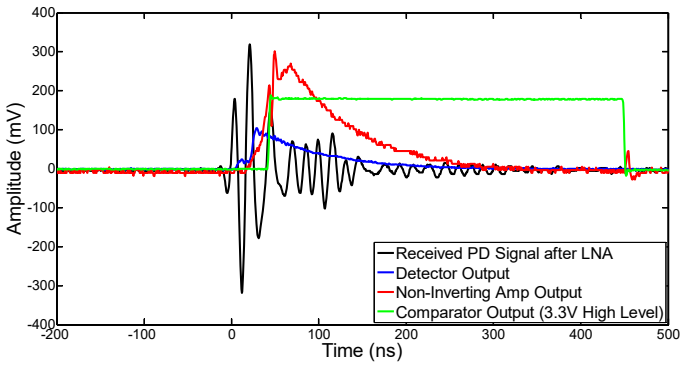

Figure 6. Emulated PD signal received by the sensor, detector output, precision high-speed amplifier output and comparator output.

The TRI, Figure 7, is also designed using composite based techniques. Q_4, R_{17}, U_5 and C_5 form a precision FET input integrator. Q_4 is resistor biased since the common-mode input voltage is a DC constant at approximately 0 V. U_6 provides DC stability by monitoring the summing point at the gate of Q_4 and comparing it to ground. The output then compensates for the V_{GS} of Q_4, in a similar fashion to that of Figure 4, and provides an overall DC offset equal to that of U_6. The resulting circuit is a high input-impedance, high-speed, precision integrator with very low DC drift between received PD signals.

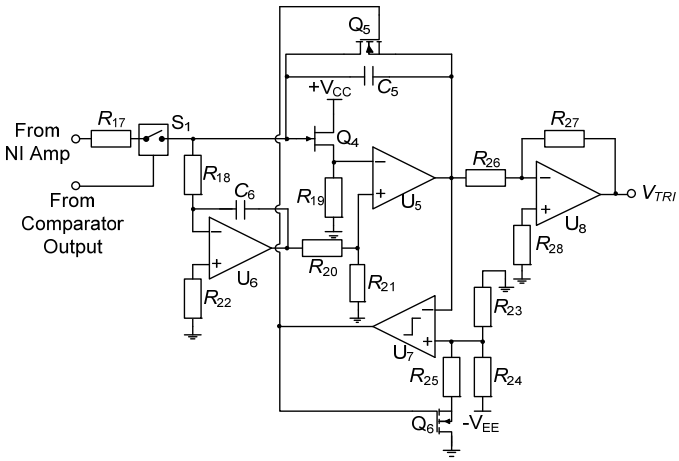

Figure 7. Precision high-speed composite TRI.

As with the precision high-speed amplifier, DC temperature drift is dependent on U_6 and is less than 0.05 µV/ºC. The entire signal conditioning circuitry consumes only 27 mW from a 3.3 V supply.

When an envelope detected PD signal is applied to the TRI (and only when such a signal is detected) the comparator closes S_1 and the TRI starts integrating. Once the received signal drops below the comparator threshold the TRI enters its hold mode and the output voltage, proportional to the energy of the received pulse, remains at a constant level. Subsequent received signals are processed in the same way, resulting in a staircase signal at the output of the TRI. When the output of the TRI reaches a threshold of -1.5 V (set by resistors R_{23} and R_{24}) comparator U_7 outputs a high level switching on Q_5. This discharges the integrator capacitor C_5 and activates Q_6 which changes the comparator threshold to approximately 0 V. This ensures capacitor C_5 is fully discharged and the integrator is reset. The inverting amplifier, U_8, inverts the negative going voltage of the TRI resulting in a positive signal and amplifies it by two, ensuring the full 0-3 V resolution of the 10-bit ADC is used. A step to the TRI output voltage can be calculated from:

$$\Delta V_{TRI} = \frac{A_{VT}}{\tau_{TRI}} \int_0^{t'} V_{DET} dt \qquad (2)$$

where ΔV_{TRI} is a step change to the TRI output voltage, and τ_{TRI}, A_{VT}, and V_{DET} are the TRI time constant (1 µs), signal conditioning unit gain and detector output voltage respectively. Since $V_{DET} = KP_{LNA}$, where P_{LNA} is the LNA

output power, the output of the signal conditioning circuitry can be related to the received PD energy by:

$$E_{LNA} = \frac{\tau_{TRI}}{KA_{VT}} \int_0^{t'} V_{DET}\, dt \tag{3}$$

where E_{LNA} is the LNA output energy for a single PD pulse. Figures 8 and 9 show the output of the TRI for a single emulated PD event and for multiple events.

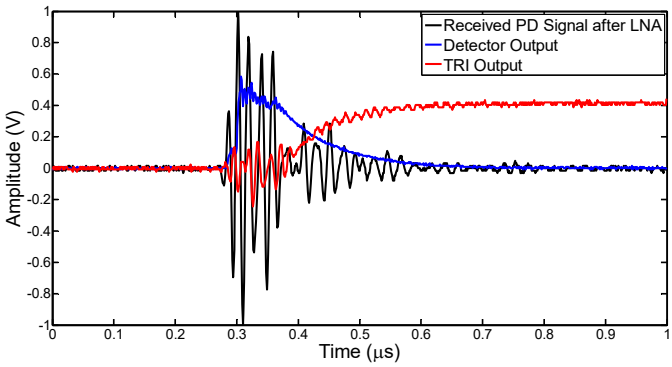

Figure 8. Received PD pulse after LNA, detector output and TRI output.

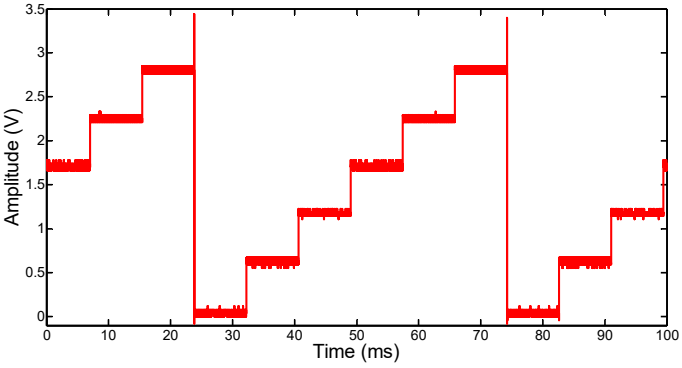

Figure 9. TRI output for multiple received PD events.

3 RESULTS

3.1 PERFORMANCE EVALUATION

To confirm the accuracy of the detector and TRI an artificial PD was generated via a floating electrode PD emulation cell and a 30 kV AC power supply, Figure 10.

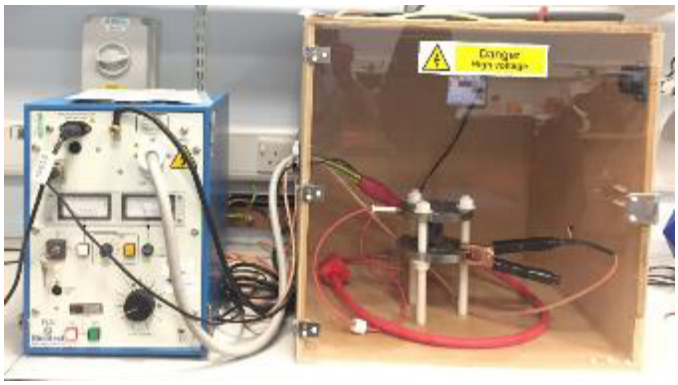

Figure 10. 30 kV power supply and floating point PD emulation cell.

The 30 kV power supply was connected to the PD emulation cell and energized at 10 kV. The resulting radiometric signal, propagated from the PD cell, was received using a dipole antenna connected to the input of the sensor under test, at a distance of 2 m from the PD source. The outputs of the LNA, detector and TRI were then measured using a digital sampling oscilloscope (DSO), Figure 11.

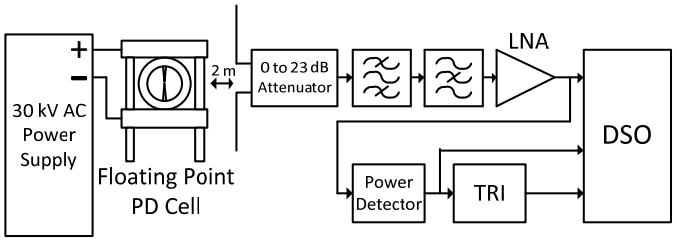

Figure 11. Configuration for indoor testing.

The received signal was attenuated using RF pads from -3 to -23 dB to simulate increasing sensor distance from the PD source. The amplified PD signal, detector output and TRI output were sampled at 2 GSa/s using a DSO. The received energy was calculated using (3) for the TRI output, whilst the amplified PD pulse and detector output were integrated digitally to find PD pulse energies using (3) and (4) respectively.

$$E_{LNA} = \Delta T \sum_{i=n}^{n} \frac{Vi^2{}_{LNA}}{R} \tag{4}$$

$$E_{DET} = \Delta T \sum_{i=n}^{n} \frac{Vi_{\,DET}}{K} \tag{5}$$

where E_{LNA} and E_{DET} are the LNA output and detector output energies, ΔT is the time between sampled data points (0.5 ns), V_{LNA} is the LNA output voltage, n is the number of samples (2000), and R is the input impedance of the sensor under test (50 Ω). Figure 12 shows the energies calculated from the amplified received PD and detector output signals, plus the sampled TRI output signal.

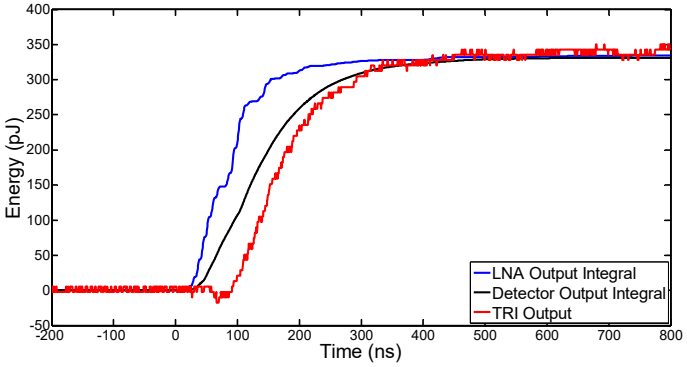

Figure 12. Integrals of the powers calculated from the amplified received PD signal, the zero bias detector output and the TRI output.

The time delay between the LNA and detector energies is due to the response of the detector causing a minor expansion to the pulse envelope. The further delay to the TRI response is due to the transient response times of the high-speed comparator and analog switch S_1, along with propagation

delays through interconnecting transmission lines and adapters. However, although delays are present between each integral, they still converge to approximately the same value. The results are shown in Figure 13 with the vertical axis plotted in dBnJ (decibels per nano-Joule). The difference between the energies inferred from the DSO measurement, detector output and TRI output are shown in Figure 14.

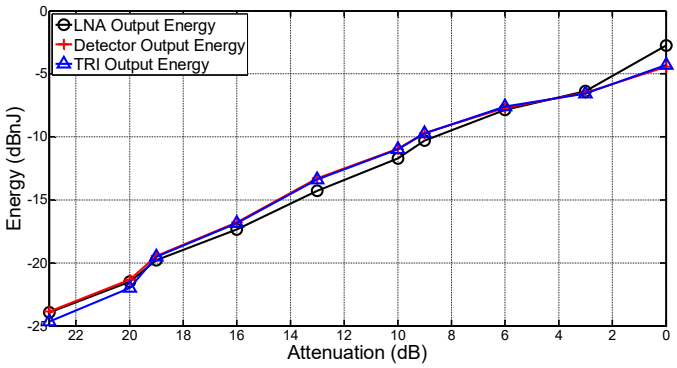

Figure 13. LNA output, detector output and TRI output energies versus attenuation.

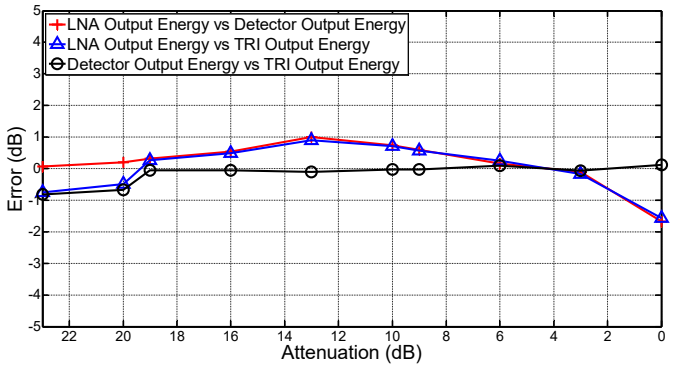

Figure 14. LNA output, detector output and TRI output error versus attenuation.

We assume the energy calculated using (4) from the DSO measurement of the LNA output signal to have the highest accuracy. The accuracy of the detector output (with respect to the LNA output) is +1.0/-1.7 dB. The accuracy of the TRI is +0.9/-1.6 dB. The difference between the detector and TRI outputs is +0.1/-0.8 dB suggesting that the error is principally due to non-linearity of the detector response, especially at high signal levels. The accuracy of the energy inferred from the TRI output has been shown to be sufficient for RSS location of PD sources to within about 1 m.

3.2 OUTDOOR DISTANCE AND LOCALIZATION ACCURACY TESTS

Further comparisons between the energy obtained through direct sampling and the TRI output were generated through outdoor testing of the sensor, and comparing the accuracy of the LNA output energy to that of the detector and TRI. A 10 nC emulated PD source was generated via a commercial HVPD pC (Pico-coulomb) calibrator, and transmitted via a dipole antenna, resulting in a narrow-band PD like pulse, Fig. 8. The sensor was then used to measure the emulated HVPD PD source from a distance of 1 to 10 m in increments of 1 m. Figure 15 shows the energies measured at a given distance, whilst Figure 16 shows the error between the energies calculated from the detector and TRI outputs compared to the energy obtained through direct sampling.

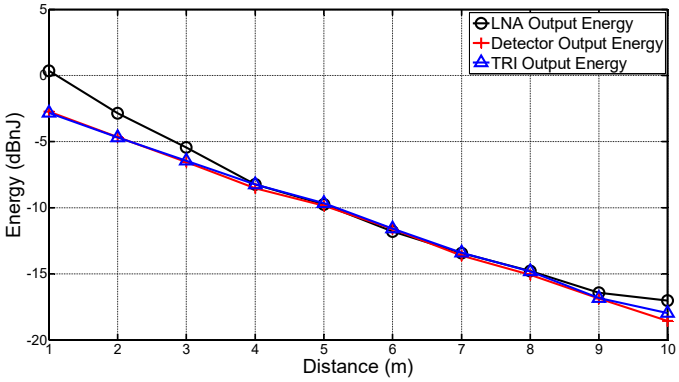

Figure 15. Outdoor measurement of an emulated 10 nC PD source at distances of 1 to 10 m.

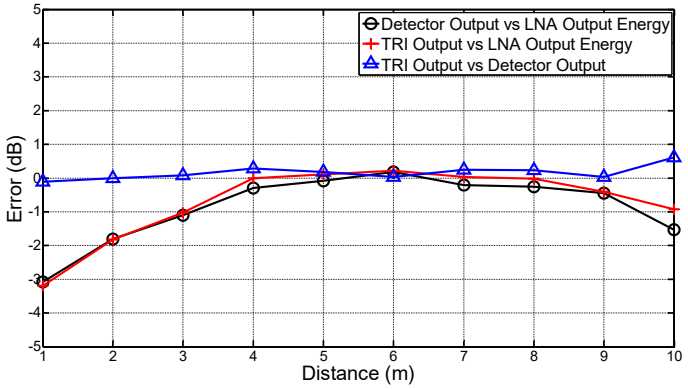

Figure 16. Errors between sampled, detector and TRI energies for the distance measurements.

The error between TRI and detector energies is between -0.1 and +0.3 dB. The error between the detector output and LNA output energies is between -0.4 and +0.2 dB beyond a distance of 4 m, whilst the error between the LNA Output energy and the TRI is between -0.4 and +0.2 dB beyond 4 m. At distances below 4 m the error increases, with an error of -3.1 and -3.2 dB at 1 m for the detector output and TRI output energies respectively, corresponding to an error in distance of approximately 1 m. This error is due to the zero-bias detector entering the transition between the square and linear responding regions, above a signal level of approximately 0 dBm.

To determine the impact of the error at distances below 4 m the accuracy of the TRI was evaluated for radiometric PD localization and compared to location estimation performed using the energy obtained through direct high-speed sampling, with the focus on the relative error between measurement techniques and not the absolute accuracy. This was performed by creating a six position 3 by 2 grid of node locations, spaced 5 m apart, Figure 17. A spacing of 5 m was used to ensure each sensor was able to receive the radiometric PD signal, since the range of the sensors is limited by the sensitivity of the detector used.

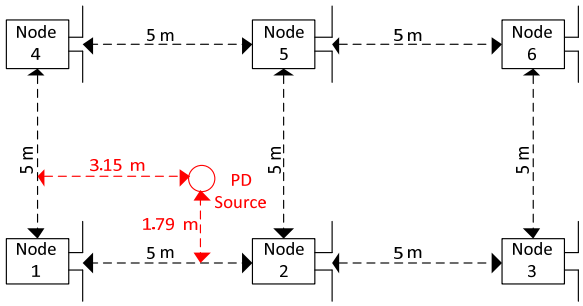

Figure 17. Outdoor PD Localization Test Sensor Layout.

The reference origin was set at Node 1. The emulated PD source was placed at x and y coordinates of 3.15 and 1.79 m. The LNA output, detector output and TRI output were recorded, at each node location from 1 to 6, using a DSO at a 2 GSa/s sample-rate. The energies were then calculated for each recorded signal using the same methods as those used for Figure 13. In order to calculate the location estimations, a simple location algorithm was implemented, derived from (5) and (6), based on RSS where the transmitted power is unknown [28]. The algorithm uses ratios of powers received from sensor pairs for location estimation.

$$R_i = R_0 - 10n\log_{10}d_i \tag{6}$$

$$\frac{d_i}{d_1} = \sqrt[n]{\frac{P_1}{P_i}} = \left(\frac{P_1}{P_i}\right)^{\frac{1}{n}} \tag{7}$$

where R_i, P_i, and d_i are the ith sensor received power in dBm, linear power in mW and distance from the PD source, R_0 is the transmitted power in dBm, n is the path-loss index, and P_1 and d_1 are the 1st sensor received power in mW and distance from the source. In free-space n is typically 2 over short distances, increasing to 4 over larger distances when grounds reflections are introduced, and increasing further if the environment has obstructions or produces multi-path propagation. The received power of the 1st sensor is used as the reference power for all other sensors. No processing was performed to improve the accuracy of the location algorithm or to resolve any multipath or scattering, to ensure that any error between the sampled, detector and TRI energies were left uncorrected; and therefore, any difference between measurement techniques was evident. In a practical installation site, the propagation environment is complex, producing a filtering effect to the radiometric PD signal, with multipath and scattering causing sufficient errors to location accuracy; therefore, a more complex location algorithm could be implemented to account for the path-loss parameters [29-31]; however, location estimation of 1 m accuracy is sufficient within a practical setting, and the filtering of the complex environment does not significantly affect the PD signal within the measurement bandwidth.

Since energy is the integral of the received power, the energy levels measured were directly inputted into the algorithm. The results were plotted for the sampled energy, and the energies calculated from the sampled detector and TRI outputs, for values of n from 1 to 7. Figure 18 shows the plotted location results whilst Figure 19 shows the distance error between the LNA output energy, and the detector and TRI output energies.

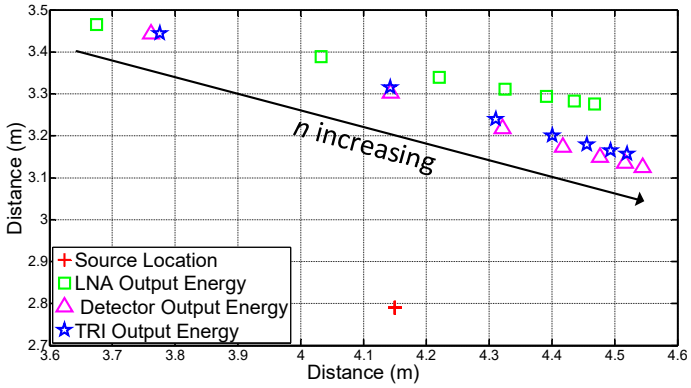

Figure 18. PD localization results obtained from the LNA output, detector output and TRI output energies for n from 1 to 7.

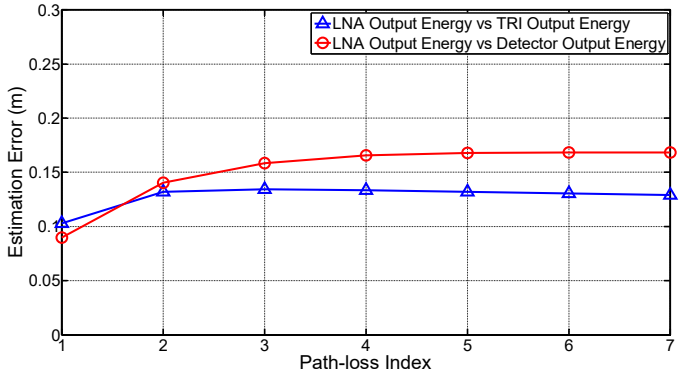

Figure 19. Errors between the LNA output energy, and detector output and TRI output energies for values of n from 1 to 7.

The estimation error is from 55 to 83 cm, 46 to 76 cm and 48 to 75 cm for the LNA output, detector output and TRI output energies respectively compared to the actual PD source location. The error in distance between the sampled energy and the TRI is between 10 and 13 cm, whilst the error between the sampled and detector energies is between 9 and 17 cm. The error between the sampled energy, and TRI and detector energies is 13 and 14 cm respectively when the path-loss index equals 2. The errors between each energy measurement technique are minor in contrast to those compared to the actual PD source location and measurement results.

4 CONCLUSION

A technique for the measurement of radiometric PD signals has been described that requires minimal power consumption and data processing. The composite TRI-based signal conditioning circuitry consumes only 27 mW, providing a low power signal processing solution for large-scale radiometric monitoring of HV insulation health in electricity substations. The measurement accuracy realized by the proposed circuit is within 1 dB for distances greater than 4 m, and within 3.2 dB below 4 m, placing the measurement accuracy of a single sensor to within 1 m. This error is sufficient for assessment and location of PD and it is acceptable considering the cost

and power reduction. Greater accuracy and distance could be secured using a detector with higher linearity and sensitivity, at an increase in power and cost. This could be performed using automatic gain control in the RF section, sub-ranging the received signal into multiple identical amplitude bands, therefore limiting the range seen by the detector whilst allowing for a higher overall dynamic range. This would allow for a greater spacing between sensor nodes, and therefore a reduction of the total number of sensors required.

ACKNOWLEDGMENT

The authors acknowledge the Engineering and Physical Sciences Research Council for their support of this work under grant EP/J015873/1.

REFERENCES

[1] High Voltage Test Techniques – Partial Discharge Measurements, International Electrotechnical Commission Standard 60270, 2000.

[2] CIGRE WG D1.33, "Guide for Electrical Partial Discharge Measurements in compliance to IEC 60270," Technical Brochure 366, Electra, vol. 60, no. 241, 2008.

[3] G. C. Stone, "Partial Discharge Diagnostics and Electrical Equipment Insulation Condition Assessment", IEEE Trans. Dielectr. Electr. Insul., vol. 12, pp. 891-903, 2005.

[4] R. Candela, A. Di Stefano, G. Fiscelli, S. F. Bononi, and L. De Rai, "A novel partial discharge detection system based on wireless technology", in *Proceedings of the AEIT Annual Conference*, 2013, pp. 1-6.

[5] P. J. Moore, I. Portugues, and I. A. Glover, "A Non-Intrusive Partial Discharge Measurement System based on RF Technology", in *Proceedings of the IEEE Power Engineering Society General Meeting*, 2003, pp. 628-633.

[6] S. Meijer, P. D. Agoris, T. J. Seitz, and T. J. W. H. Hermans, "Condition assessment of power cable accessories using advanced VHF/UHF PD radio-frequency techniques," in IEEE Trans. Dielectr. Electr. Insul., vol. 18, no. 2, pp. 444-455, 2011.

[7] P. Kakeeto, M. Judd, J. Pearson, and D. Templeton, "Experimental investigation of positional accuracy for UHF partial discharge location", in *Proceedings of the IEEE International Conference on Condition Monitoring and Diagnosis,* 2008, pp. 1070-1073, 2008.

[8] Y. Tian, B. Qi, R. Zhuo, M. Fu, and C. Li, "Locating partial discharge source occurring on transformer bushing by using the improved TDOA method", in *Proceedings of the IEEE International Conference on Condition Monitoring and Diagnosis*, 2016, pp. 144-147.

[9] H. H. Sinaga, B. T. Phung, and T. R. Blackburn, "Partial Discharge Localization in Transformers Using UHF Detection Method", IEEE Trans. Dielectr. Electr. Insul., vol. 19, pp. 1891-1900, 2012.

[10] J. Vedral, and M. Kriz, "Signal Processing in Partial Discharge Measurement", Metrology and Measurement Systems, vol. 17, pp. 55-64, 2010.

[11] A. J. Reid, M. D. Judd, R. A. Fouracre, B. G. Stewart and D. M. Hepburn, "Simultaneous measurement of partial discharges using IEC60270 and radio-frequency techniques," in IEEE Trans. Dielectr. Electr. Insul., vol. 18, pp. 444-455, 2011.

[12] A. J. Reid, M. D. Judd, B. G. Stewart, R. A. Fouracre, and S. Venkatesan, "Correlation between RF energy and IEC60270 apparent charge for selected partial discharge source geometries", in *Proceedings of 15th International Symposium on High Voltage Engineering*, 2007.

[13] A. J. Reid, M. D. Judd, B. G. Stewart, and R. A. Fouracre, "Comparing IEC60270 and RF partial discharge patterns", in *Proceedings of the IEEE International Conference on Condition Monitoring and Diagnosis*, 2008, pp. 89-92.

[14] W. Huang, C. Zhang, M. Dong, and J. Zhou, "Research on Partial Discharge Monitoring System of Switchgear Based on Wireless Distributed TEV Sensors", in *Proceedings of the 1st International Conference on Electrical Materials and Power Equipment*, 2017, pp. 647-650.

[15] E. T. Iorkyase, C. Tachtatzis, R. C. Atkinson, and I. A. Glover, "Localisation of Partial Discharge Sources using Radio Fingerprinting Technique", in *Proceedings of the Loughborough Antennas and Propagation Conference*, 2015, pp. 1-5.

[16] W. Zhang, K. Bi, Z. Li, L. Luo, G. Sheng, and X. Jiang, "RSSI Fingerprinting-based UHF Partial Discharge Localization Technology", in *Proceedings of the IEEE PES Asia-Pacific Power and Energy Engineering Conference*, 2016, pp. 1364-1367.

[17] P. C. Baker, M. D. Judd, and S. D. J. McArthur, "A Frequency-based RF Partial Discharge Detector for Low-power Wireless Sensing", IEEE Trans. Dielectr. Electr. Insul., vol. 17, pp. 133-140, 2010.

[18] J. M. R. De Souza Neto, J. S. Da Rocha Neto, E. C. T. Macedo, I. A. Glover, and M. D. Judd, "An envelope detector as a trading cost technique for radiometric partial discharge detection", in *Proceedings of the IEEE International Instrumentation and Measurement Technology Conference*, 2014, pp. 1584-1589.

[19] Y. Zhang, J. M. Neto, D. Upton, A. Jaber, U. Khan, B. Saeed, H. Ahmed, P. Mather, R. Atkinson, J. S. Neto, M. F. Q. Viera, P. Lazaridis, and I. A. Glover, "Radiometric monitoring system for partial discharge detection in substation", in *Proceedings of the 1st URSI Atlantic Radio Science Conference,* 2015, pp. 1-1.

[20] Y. Zhang, D. Upton, A. Jaber, H. Ahmed, B. Saeed, P. Mather, P. Lazaridis, A. Mopty, C. Tachtatzis, R. Atkinson, M. Judd, M. F. Q. Viera, and I. A. Glover, "Radiometric wireless sensor network monitoring of partial discharge sources in electrical substations", Hindawi Int'l. J. Distrib. Sensor Networks, vol. 2015, pp. 1-9, 2015.

[21] D. W. Upton, B. I. Saeed, U. Khan, A. Jaber, H. Mohamed, K. Mistry, P. J. Mather, P. Lazaridis, M. F. Q. Vieira, R. Atkinson, C. Tachtatzis, E. Iorkyase, M. Judd, and I. A. Glover, "Wireless Sensor Network for Radiometric Detection and Assessment of Partial Discharge in HV Equipment", in *Proceedings of the 32nd URSI General Assembly and Scientific Symposium*, 2017, pp. 1-4.

[22] S. Xiao, P. J. Moore, and M. Judd, "Investigating the Assessment of Insulation Integrity Using Radiometric Partial Discharge Measurement", in *Proceedings of the International Conference on Sustainable Power Generation and Supply*, 2009, pp. 1-7.

[23] A. A. Jaber, P. I. Lazaridis, M. Moradzadeh, I. A. Glover, Z. D. Zaharis, M. F. Q. Vieira, M. D. Judd, and R. C. Atkinson, "Calibration of Free-Space Radiometric Partial Discharge Measurements" IEEE Trans. Dielectr. Electr. Insul., vol. 24, pp. 3004-3014, 2017.

[24] Agilent Technologies, Appl. Note 988, pp. 1-4.

[25] Linear-Technology, Appl. Note 21, pp. 1-3.

[26] Linear-Technology, Appl. Note 47, pp. 32-25.

[27] R. C. Jaeger and T. N. Blalock, *Microelectronic Circuit Design,* 4th ed., McGraw-Hill: New York, pp. 1073-1074, 2011.

[28] Y. Liu, Z. Yang, X. Wang, and L. Jian, "Location, Localization, and Localizability", Journal of Computer Science and Technology, Vol. 25, pp. 274-297, 2010.

[29] Y. Xu, J. Zhou, and P. Zhang, "RSS-Based Source Localization When Path-Loss Model Parameters are unknown", IEEE Communications Letters, vol. 18, pp. 1055-1058, June 2014.

[30] J. M. Fresno, G. Robles, J. M. Martinez-Tarifa, and B. G. Stewart, "Survey on the performance of source localization algorithms", Sensors, vol. 17, pp. 1-25, 2017.

[31] E. T. Iorkyase, C. Tachtatzis, P. Lazaridis, I. A. Glover, and R. C. Atkinson, "Radio Location of Partial Discharge Sources: A Support Vector Regression Approach", IET Science, Measurement & Technology, pp. 1-9, 2017.

David W. Upton was born in Oldham, UK, in 1983. He received the B.Eng.(Hons.) degree in Electronic Engineering from the University of Huddersfield, UK, in 2013. He is currently working towards the Ph.D. degree in electronic engineering at the University of Huddersfield. Since 2016 he has been a research assistant with the School of Computing and Engineering at the University of Huddersfield. His research interests include wireless partial discharge sensors, analog signal processing for pulsed signals, precision and high speed analog electronics, and integrated analog design. Mr. Upton was the recipient of the IET Gerald David Memorial Prize for an outstanding mature student in 2013, and was awarded the Vice-Chancellor scholarship by the University of Huddersfield for his PhD degree. Mr Upton is a member of the IET.

Bakhtiar I. Saeed received the B.Eng. degree in computer and control systems engineering from the University of Technology, Baghdad, Iraq in 1992 and the M.Sc. degree in computer systems and networking from the University of Greenwich, UK in 2009. He received the Ph.D. degree from the University of Huddersfield, UK in 2014. From 1993 to 2008, he worked as a lecturer at the Suleimany Computer Science Institute and the Technical Institute of Suleimany, in Iraqi Kurdistan Region. Since 2015, he has been a post-doctoral researcher with the School of Computing and Engineering at the University of Huddersfield. His research interests include partial discharge, fuzzy logic controllers, embedded systems, IoT, intelligent sensors, and wireless sensor networks. Dr. Saeed is a member of the IET, the British Computer Society (BCS), the Higher Education Academy (HEA) and the Kurdistan Engineering Union.

Peter J. Mather received the B.Eng.(Hons.) degree in Electrical and Electronic Engineering1990and the Ph.D. degree from the University of Huddersfield, UK, in 1990 and 1995 respectively. After completing post-doctoral research in mixed signal test techniques, he was a senior mixed signal IC design engineer. He is currently a senior lecturer at the University of Huddersfield, UK. His research interests include coding scheme implementation and non-linear-based measurement. Dr Mather is a fellow of the HEA and is a member of the IET.

Martin J. N. Sibley received the B.Sc.(Hons.) degree in electrical engineering and the Ph.D. degree from Huddersfield Polytechnic, Huddersfield, U.K., in 1981 and 1984, respectively. From 1981 to 1984, he was at Huddersfield Polytechnic, where he was sponsored by British Telecom Research Laboratories to research the design of common-collector input preamplifiers for use in optical receivers. This study led to the first preamplifier design in IC. He is currently a Reader at the University of Huddersfield, Huddersfield. His current research interests include pulse-position modulation, preamplifier design for optical receivers, optical wireless LANs, and free-space optical links.

Pavlos I. Lazaridis received the BSc degree in Electrical Engineering from Aristotle University of Thessaloniki, Greece, in 1990, the MSc in Electronics from Université Pierre & Marie Curie, Paris 6, France in 1992 and the PhD from ENST Paris and Paris 6, in 1996. From 1991 to 1996, he was involved with research for France Télécom and teaching at ENST Paris. In 1997, he became Head of the Antennas and Propagation Laboratory, TDF-C2R Metz. From 1998 to 2002 he was senior Examiner at the European Patent Office (EPO), Den Haag, the Netherlands. From 2002 to 2014 he was involved with teaching and research at the ATEI of Thessaloniki, Greece and Brunel University West London. He is currently a Reader in Electronic and Electrical Engineering at the University of Huddersfield, United Kingdom, member of the IET, and a Fellow of the Higher Education Academy.

Keyur K. Mistry received the B.Tech degree in electronics and telecommunication engineering from the NMIMS University, Mumbai, India in 2015 and the Master's degree in electronics and communications engineering from the University of Huddersfield, UK, in 2016. He is currently working towards the Ph.D. degree in electronics and communications engineering. His research interests include antenna design and measurements, wireless partial discharge sensors, UHD TV broadcasting and developing optimization algorithms. He was awarded the Vice-Chancellor scholarship by the University of Huddersfield for his PhD degree. He was also recipient of the 1st prize for Best design for proof of concept design competition organized by ICE/Honeypot in 2016.

Ian A. Glover is currently Professor of Radio Science & Wireless System Engineering, and Head of the Department of Engineering and Technology, at the University of Huddersfield, UK. Ian's principal research interest is in the application of radiometric and wireless communication methods to insulation condition monitoring and asset management of high-voltage plant in the future smart grid. His other interests include classical radio propagation for applications ranging from satellite communication, mobile communications, radar and wireless sensor networks. He is the author, with Peter Grant, of Digital Communications (1998, 2004, 2008) published by Pearson and the editor (with Peter Shepherd and Stephen Pennock) of Microwave Devices, Circuits and Subsystems for Communications Engineering (2005) published by Wiley. Ian Glover is a member of the IET, IEEE and IoP, and is a Fellow of the Academy of Higher Education.

Flavio Torres Filho received the B.E. (2009), MSc (2011) and DSc. (2015) in electrical engineering, all from the Federal University of Campina Grande (UFCG) in the state of Paraiba in Brazil. His formation background is on Automation, Control and Computer Engineering. He is currently a senior lectureer at the Federal Institute of Paraíba (IFPB-Brazil) where he teaches and researches in the fields of Industrial Automation and Computer Engineering. Since 2008 he has been an active member of the research team at the Man Machine Interface Laboratory (LIHM) at UFCG.

Christos Tachtatzis (M'05) received the BEng (Hons) degree in communication systems engineering from the University of Portsmouth, UK in 2001. He received the MSc and PhD degrees in communications, control and digital signal processing and electronic and electrical engineering from the University of Strathclyde, Glasgow, UK in 2002 and 2008 respectively. From 2008 to 2016 he held postdoctoral researcher positions at the University of Strathclyde, UK and Letterkenny Institute of Technology, Republic of Ireland. Since 2016, he is a Lecturer at the Department of Electronic and Electrical Engineering. His research interests include distributed sensing, communication networks, edge computing analytics, computer vision and artificial intelligence. Dr Tachtatzis received the Strathclyde Chancellor's Fellow award in 2016 and is a member of the IET.

Robert C Atkinson is a Senior Lecturer in the Department of Electronic and Electrical Engineering, University of Strathclyde. He has applied a range of signal processing and machine learning algorithms to a range of fields as diverse as: radiolocation of partial discharge, intrusion detection systems, 4G handover optimization, game theory applied to radio access network selection, prognostics for gearboxes, condition-based maintenance of water pumps, internet of things, smart cities, smart buildings, and image analysis for pharmaceutical crystals. He is the author of over 80 scientific papers, published in internationally recognized conferences and journals. He is a Member of the IET and a Senior Member of the IEEE.

Martin D. Judd (M'2002-SM'2004) is Technical Director of High Frequency Diagnostics Ltd, based in Glasgow, Scotland. He received the B.Eng.(Hons.) degree in Electronic Engineering from the University of Hull, UK, in 1985. He worked in industry for 8 years, with Marconi Electronic Devices and then with EEV Ltd. Martin received the Ph.D. degree in Electronic Engineering from the University of Strathclyde, UK, in 1996. He has worked extensively on UHF partial discharge location techniques for power transformers and was latterly Professor of High Voltage Technologies at the University of Strathclyde, where he managed the High Voltage Research Laboratory. In 2014 he founded High Frequency Diagnostics, a specialist consultancy business that works in partnership with companies developing new electromagnetic wave sensor technologies and applications.